A Real-Time Embedded System Designed for NILM Studies with A Novel Competitive Decision Process Algorithm

Said Mahmut ÇINAR[1*], **Rasim DOĞAN**[2] , **Emre AKARSLAN**[3]

[1,2,3]Electrical Engineering Department, Engineering Faculty, Afyon Kocatepe University, Afyonkarahisar, Turkey,

ORCID iD: [1]https://orcid.org/0000-0002-6810-1575 [2]https://orcid.org/0000-0003-2122-9528 [3]https://orcid.org/0000-0002-5918-7266

Abstract: This paper investigates the determination of any load or load combination in a power system at any instant. This process needs measurement at the main electric utility service entry of a house called Non-Intrusive. To accurately identify, Total Harmonic Distortion, RMS and third harmonic currents, and power consumption are considered fingerprints of loads. Based on these fingerprints, an algorithm called the Competitive Decision Process is developed and integrated into an embedded system. This algorithm has a two-level decision mechanism. In the first stage, the winner loads with the highest similarity scores from each feature are determined, and the loads with a higher similarity score than 90 move to the second stage to be evaluated. Loads that do not pass the first stage in all features are not considered for the next one. In the second stage, the scores from each feature of the loads passed to this stage are summed, and the load with the highest score is determined. It is experimentally validated that the method significantly detects correct load or load combinations for six residential appliances. Fifty-six type-tests are performed, and each type-test contains ten measurements. As a result, a total success rate of over 97 percent is obtained in all metrics.

Key words: Harmonic analysis, Non-intrusive load identification, Residential appliances, embedded system, similarity score

1. Introduction

This paper focuses on the determination and identification of loads present at any moment in a power system. This method, also known as Non-intrusive load monitoring (NILM), was first proposed by Hart [1][2]. He declared that appliances operated in the house could be identified from the measurement captured at the utility side. Only active and reactive power (P and Q) measurements are recorded during 5-second intervals, and loads are determined by a clustering algorithm. Although simple, the method requires continuous recording, and inaccurate identifications are possible for similar loads. Significant progress has been made over time using very different approaches and features in the studies in this field, which started with Hart.

In [3], an approach is proposed to identify harmonic source loads for industrial users. The study monitors current and voltage signals, and the integrated equivalent impedance is calculated. Then, complex local mean decomposition (CLMD) and complex fast independent component analysis (CFICA) are used to separate the equivalent impedance signal. The results illustrate that the approach is suitable for industrial users. [4] proposes a rule-based approach for load identification. The Fourier Transform of the current signal is employed, and some statistical features, such as minimum, maximum, standard deviation, etc., are extracted from this signal. Then,

---

*Correspondence: smcinar@gmail.com

the appliances are classified according to the rule table constructed from the boundaries of each load appliance in terms of extracted features. Over 90% accuracy is obtained in this study. [5] also uses statistical features for low-sampling NILM systems. An event detection-based structure is designed, and a sliding window (SW) based algorithm that monitors the statistical properties of the aggregated load data is employed. Around 90% of performance is obtained in terms of precision and recall metrics. In [6], a Raspberry Pi-based system is designed for real-time non-intrusive load monitoring. In the designed system, current and voltage signals are collected, and some features such as active, reactive, and apparent power and RMS values of current and voltage are calculated from these signals. The Fractional Hidden Markov model and an automatic state detection algorithm are combined for load disaggregation. [7] also designs a Raspberry Pi-based system that uses active, reactive, and apparent power. Some statistical approaches, such as the Hidden Markov Model (HMM) [8], The Factorial Hidden Markov Model (FHMM) [9], and Additive Factorial Approximate Maximum A-Posteriori (AFAMAP) [10] are also used in different studies with power signal features. The differences by converting the time domain to the frequency domain for load currents are investigated, and the change in the current waveform is traced and isolated in [11]. The isolated current frequency spectrum is compared with each load frequency spectrum in the database, and load disaggregation success is remarkable. The linear and nonlinear properties of loads were investigated from the harmonic point of view and presented that harmonic components and active and reactive powers could be used as distinguishing features in their analysis [12][13].

[14] proposes a transfer learning-based approach for NILM studies. Some features such as power factor, power, and maximum power index are used as features, and the LSTM (Long Short-Term Memory) method is used for feature extraction. Then, the probabilistic neural network is employed to classify the appliances. It is shown that the proposed method can work on limited data. [15] also uses LSTM with power information. The target dataset is employed to pre-train the network in the first stage, while supervised downstream tasks are used to fine-tune the pre-trained network. In the last stage, load disaggregation is performed by the fine-tuned network. In [16], 1st, 3rd, 5th, 7th, and 9th harmonic currents, the angles of these signals and THD (total harmonic distortion) information are employed as features, and their importance is investigated. Then, the radial basis function and Elman neural network methods are used to classify the appliance. In [17], the current and voltage signals are transformed into structured images representing the relation between load types and features. Then, convolutional neural networks and combined Support Vector Machines are employed for the classification of the images and data. The results obtained show that the proposed method is more successful than many existing conventional methods. [18] also proposes a deep learning approach called a physics-informed time-aware neural network method for industrial loads. In the study, active, reactive, and apparent power are employed as features, and the success of the approach is compared with the conventional deep learning approach. The experimental results on real-world industrial data illustrate the success of the approach.

As seen in the existing literature, many NILM studies consider events, such as edge, sequence, duration, etc., that occurred in power measurements [19]–[21]. Since the method requires a very long measurement time to capture the necessary events, any interruption during the process may affect the accuracy. Common features of all these studies include the search for a distinctive feature in determining each of the loads and determining loads based on these features. Some have looked at macroscopic features (such as ON/OFF) and others microscopic features (such as transients and harmonics) [22]–[25]. However, it is common in most studies that the best detection method is the investigation of microscopic properties.

Contrary to steady-state measurements, transient currents that occurred during the energizing and de-energizing moments of each appliance are considered in determining load [26, 27]. In addition, both steady-

state and transient currents are evaluated to estimate the load [28]. However, it is hard to detect transients when energized or de-energized low-power loads in high-power environments. Further, event-based strategies require tracking and storing the previous state information; in case of any loss of this information, many of the approaches fail. Machine learning and artificial intelligence methods are generally preferred in such studies when classifying appliances. However, the computational complexity of such methods is relatively high, and depending on the training section and models, the success rate of the method changes significantly.

This study proposes a novel method called the Competitive Decision Process (CDP). The method has a two-level decision mechanism. In the first level, all winner loads with a higher similarity score (SS) than 90 are determined for each feature and sent to the second level for the final decision. The final winner is selected according to a total score in the second level. In this way, high identification performance can be achieved by considering only combinations of high importance while reducing the complexity of the process. The proposed approach does not require a training stage, and the computational complexity is reduced; therefore, it gets advantages in real-time applications. In the decision process, only one cycle current for individual appliances is used as reference signals. For combinations, reference signals are obtained from individual appliance measurements, and SS values are calculated for all possible appliance/appliance combinations. The method uses THD, power consumption, RMS, and third harmonic current as features. In order to operate and control the whole process, an STM®-based embedded system is designed. Therefore, a fast, accurate, and autonomous system is presented. Also, it does not require continuous and long measurements, so the predictions are not affected by any failures in the system during data acquisition. The study includes 560 measurements, and 547 (97.67%) are correctly identified with only one-period measurement. The method is validated by experiments. Results are presented and discussed in the text.

The paper is organized as implementation steps, and details of the embedded system are demonstrated in Section 2. Features that are used in the selection criteria are explained in Section 3. The competitive decision process and calculations of the proposed method are explained in Section 4. Experimental results and discussions are illustrated in Section 5, and the conclusions of the paper are presented in Section 6.

2. Implementation Steps and Details

In this section, the experimental setup, architecture of the embedded system, and data acquisition interface of the real-time load identification system are presented.

2.1. Experimental setup

The experimental setup (see Fig. 1) consists of current and voltage probes that measure the current and voltage of the power line, signal conditioning circuits adapted to the probes' output voltages to the microcontroller ADC (analog-digital converter) inputs, a development board, and a user interface that performs the monitoring and recording of the test results.

Pintek DP 25 voltage probe and Fluke 80i-110s current probe are used for corresponding measurements. Output signals are multiplied by 10 for current and 200 for voltage calibration. They are also protected from noise with galvanic isolation between the power line and the signal conditioning circuit. Signal conditioning circuits are designed to match the probe outputs to the ADC input level of the development board. These circuits perform two basic functions: scaling and adding an offset of probe outputs.

The STM32F4 Discovery board is preferred as the development board. There is an STM32F407VGT6 microcontroller with a 32-bit ARM® Cortex®-M4 core, frequency up to 168 MHz, 1-Mbyte flash memory, and

1   192-Kbyte RAM (random access memory) on the discovery board. This microcontroller is equipped with a single-
2   precision floating-point unit (FPU), which supports all ARM® single-precision data-processing instructions and
3   data types.

4   The user interface is designed on the MATLAB/Simulink development platform. It performs two primary
5   functions, such as displaying the data received from the microcontroller and saving them to the MATLAB
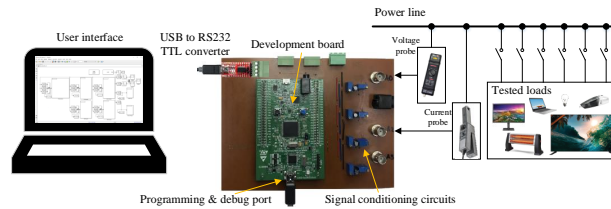6   workspace.

Figure 1. Experimental setup of the real-time load identification system.

7   **2.2. The architecture of the embedded system**

8   Model-based design (MBD) has many advantages in embedded system design, such as rapid prototyping,
9   simplification of debugging processes, modular design, and avoidance of manual code writing and coding errors
10 that may occur in this process.

11   The powerful, efficient, modular, and successful MBD must be separated into logical partitions. Therefore,
12 the study divides the MBD into four logic components: the tested loads, voltage and current probes and their
13 signal conditioning circuits, the microcontroller, and the user interface (see Fig. 2).

14   The microcontroller continuously samples the current and voltage signals to take 512 samples per period,
15 buffers them in memory, runs the load recognition algorithm once a second, and sends the results to the user
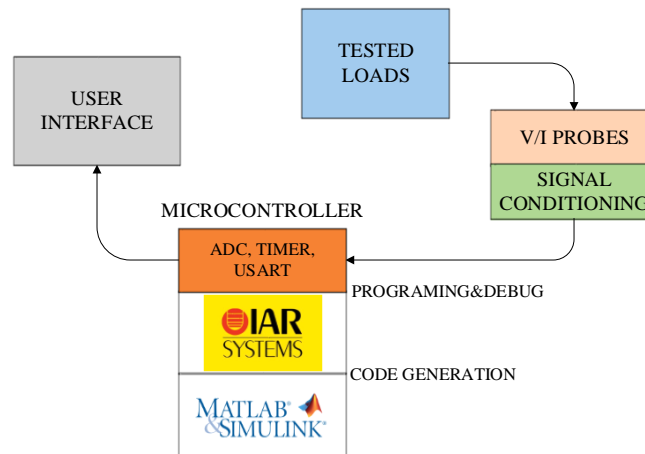16 interface as detailed explained below.

Figure 2. Partitioning the MBD.

The ADC unit is triggered with a timer with a frequency of 25,6 kHz so that 512 samples can be taken per period for sampling V/I signals. Data is buffered into RAM with the direct memory access (DMA) module when the analog conversion is completed. Then, the load identification algorithm is executed and buffers the results to the RAM with a one-second interval. Finally, the buffered data is sent to the interface via the USART (Universal Synchronous Asynchronous Receiver Transmitter) unit supported by the DMA unit.

3. Features of Load Identification

The literature presents loads that have unique features to separate them. Although features are the most crucial part of NILM studies, the key idea is to identify loads with the minimum number of features to mitigate complexity and increase accuracy. Therefore, several experiments are performed to investigate the distinctiveness and determine features.

Appliances are evaluated in three classes: ON/OFF, finite state machine (FSM), and continuously variable [1]. While a single operating mode exists in the ON/OFF class, multiple operating modes exist in the FSM class, such as the washing machine's rinsing, drying, and spinning modes. In each mode, the transition occurs in a step increase or decrease, and each can be considered a different load. In the continuously variable class, the change in load consumption is not a consistent step but a continuously variable consumption situation (light dimmers, sewing machines, etc.). Thus, six residential appliances in the ON/OFF class are selected for experiments and presented in Table 1, including their nominal powers and initials. Please note that initials will be used in the study for the corresponding loads.

Three experiments are conducted for the selection of features. The first experiment is performed with LC and HL in a single case. The harmonic distribution of LC and HL is presented in Fig. 3 and Fig. 4, respectively. The nominal power of LC is 65W, and HL is 70W. In addition, the total harmonic distortion of current (THD_I), which will be described in the next section, is 190% and 4%, respectively. Although they have low power consumption and similar RMS currents, their third harmonic currents have distinctiveness, as seen in Fig. 3 and Fig. 4. Thus, these two loads could be separated by their THD_I's and the third harmonic currents.

Table 1. Loads in experiments.

Appliances	Initials	Nominal Power (W)
Vacuum Cleaner	VC	1000
Halogen Light	HL	70
Heater	HE	600
Laptop Charger	LC	65
Monitor	MO	25
LCD Television	TV	21

The second experiment is performed with LC and MO. They are expected to have similar features since both have power converter units, e.g., AC-DC and DC-DC, and their harmonic distributions are presented in Fig. 3 for LC and Fig. 5 for MO. In comparing both figures, it is clearly seen that they have similar harmonic distribution and THDI. However, the RMS current and power consumption of LC are almost three times higher than MO. Thus, they differ from power and RMS current, although they show similarities regarding harmonic distribution.

LC and MO are operated together (multiple load case) for the third experiment, and the harmonic distribution is presented in Fig. 6. The fundamental current of multiple operations is higher than that consumed
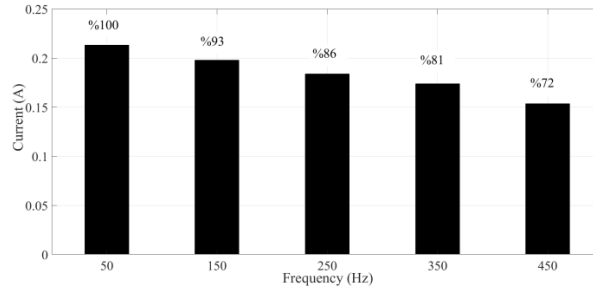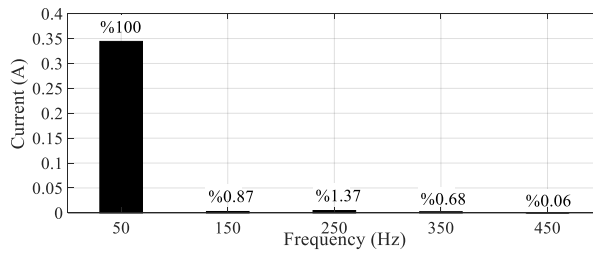
Figure 3. Harmonic distribution of LC current.

Figure 4. Harmonic distribution of HL current.
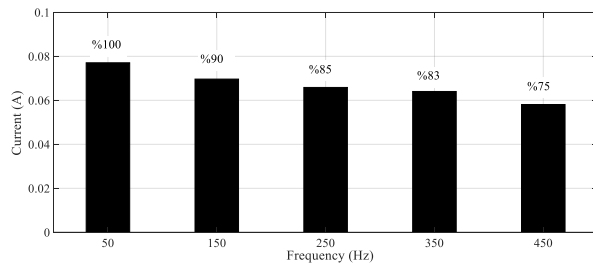

Figure 5. Harmonic distribution of MO current.

by each of their single case operations. In addition, THD_I (180%) is also less than their individual cases. However, the harmonic current distribution demonstrates similarities for both. The fundamental current of both loads is at most 0.22A. Thus, it is seen that the load presented in Fig. 6 is not only LC or MO. It should be multiple load cases, so LC-MO (90W) and HL-MO (95W) are two options based on their power consumption. For the HL-MO case, the third harmonic current would be much less than 90% (see Fig.7). However, for the LC-MO case, the third harmonic current would be around 90% because both have the same harmonic current concerning their fundamental currents. Hence, all results indicate that LC and MO are operated together after all features are considered.

The distinctiveness of the 5th, 7th, and 9th harmonics is lower than the 3rd one, although these harmonic currents have a higher effect, as indicated in [16]. Therefore, harmonics higher than 3rd one are not considered.

These experiments demonstrate that power consumption, RMS current, THD_I, and the third harmonic current have sufficient and critical information for loads. However, the acquisition of each data and their correct interpretations are the most critical factors that will increase the accuracy of the method applied. It will be explained in the next section.
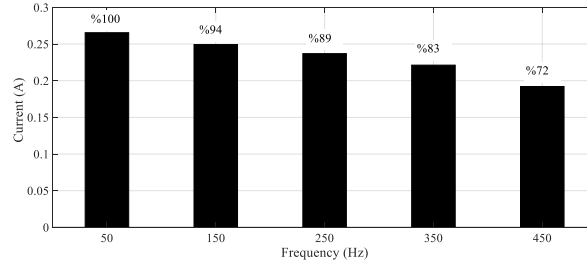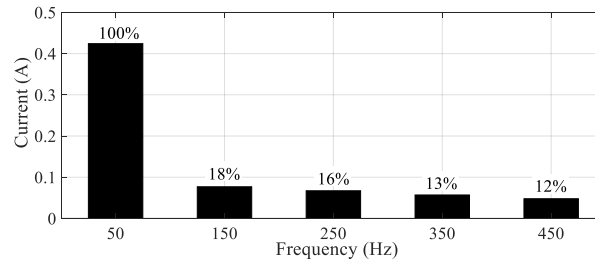

Figure 6. Harmonic analysis of MO & LC current.

Figure 7. Harmonic analysis of MO & HL current.

4. Competitive Decision Process

This study proposes a new method called the Competitive Decision Process (CDP). The proposed method only needs a one-cycle current and voltage measurement for each individual load to store in the database as a reference. One of the most important advantages of the method is that it does not require a training stage and continuous measurement. The proposed method utilizes the similarity score metric introduced in [29] while deciding, and it has a two-level decision process to identify the residential load or loads used in the experiments. It can identify both individual loads and load combinations. In the first level of this approach, similarity scores belonging to each feature are calculated by using measured signal and reference signals, as explained in detail in the following section, for all possible combinations. It should be noted that one-period reference signals are required only for individual loads, and reference signals for combination loads are not needed. The steady state measurements are used in calculation of the similarity score metric and then the winner/winners with a similarity score above 90 are determined. The reason is that there are deviations due to various reasons (noise, voltage fluctuations, etc.) in the different measurements of the same load. Since they remained in the band of about 10%, the value of 90 was considered appropriate as the threshold level for this study and is applied. In this way, it is aimed to create a stronger decision mechanism where weak relationships are ignored and only strong features are considered. In the second stage, only the winner payload combinations selected for each

feature in the first stage are considered. A final score value is obtained by summing the scores from each feature for each load combination that moves to the second stage. The highest score load combination (final winner) is assigned as the selected combination. If a load combination enters the second stage with a score higher than 90 for each used feature, the probability of that load combination being selected will be relatively high. Likewise, suppose a load combination is chosen with a high score from one feature but not from another. In that case, the probability of the highest final score will decrease since no value will come from that feature (zero). In this way, not only a more robust method has been created, but also measurement instabilities that may arise from the hardware are prevented from negatively affecting the decision. Furthermore, the computational complexity of the approach is thus reduced, as some load/load combinations are excluded from the calculation and no calculations are performed for them. One advantage of the approach is that identification can be performed any time without needing previous state information, which differs from the event-based methods. In other words, continuous measurements are optional. In this way, the storage space required to store the previous state information in embedded system applications is saved, and the loss of the previous state information does not have a negative impact on the identification performance (in event-based methods, this negatively affects the identification performance). In addition, the steady-state, the longest part of the load, has been considered in the paper since the transient effect is absorbed quickly.

After measurements, SS, which ranges from 0 to 100 for each feature, calculations are initiated. Power consumption, RMS current, THD_I, and third harmonic current are selected and employed as features during analyses. So, the load combinations with higher scores than 90 are determined for each. In the second level, the sum of SSs is calculated for loads past this stage. Then, the measured load is identified as the reconstructed load with the highest SS. Therefore, all SS calculations are described below to perform the load identification process.

4.1. Power SS

Power consumption calculated as in (1) is the most common evaluation feature for NILM studies.

$$Pu = \frac{1}{T} \int i(t)v(t)d(t). \tag{1}$$

where, P_u is the power consumption of an unknown load, and $i(t)$ and $v(t)$ are the instantaneous current and voltage measurements, respectively. To determine the SS, reconstructed power (P_{RC}) for each type-test should be calculated and compared to P_u. The reconstruction process starts with calculating each single-load power consumption for each type-test and ends with their sum. Then, SS is calculated as in (2).

$$P_{ss} = \begin{cases} 100 * \frac{P_{RC}}{P_u}, & P_{RC} < P_u. \\ 100 * \frac{P_u}{P_{RC}}, & P_u < P_{RC}. \end{cases} \tag{2}$$

where, P_{ss} is the similarity score of power consumption. Then, higher scores than 90 are considered for the second level.

4.2. RMS Current SS

RMS current is another feature to be used for the identification, calculated as in (3).

$$I_{rms-u} = \sqrt{\frac{1}{T} \int \sum i(t)^2 dt} \tag{3}$$

2   where, I_{rms-u} is the RMS current of the measured (unknown) load, and $i(t)$ is the instantaneous current.

3   The SS of RMS current, I_{rms-ss}, is calculated in (4).

$$I_{rms-ss} = \begin{cases} 100 * \frac{I_{rms-rc}}{I_{rms-u}}, & I_{rms-rc} < I_{rms-u}. \\ 100 * \frac{I_{rms-u}}{I_{rms-rc}}, & I_{rms-u} < I_{rms-rc}. \end{cases} \tag{4}$$

4   where I_{rms-rc} is the reconstructed RMS current for any possible cases. All possible combinations of

5   loads are considered to find the closest I_{rms-rc} to I_{rms-u}. Therefore, I_{rms-rc} is presented in (5) based on

6   Kirchhoff's current law.

$$I_{rms-rc} = \sqrt{\frac{1}{T} \int \sum_j i_j(t)^2 dt} \tag{5}$$

7   where, $i_j(t)$ is the sum of instantaneous currents for each corresponding load located in the database.

8   For example, if we consider the load combination of MO and TV, the $i_j(t)$ is equal to the sum of $i_{mo}(t)$ and

9   $i_{tv}(t)$.

10   **4.3. THD SS**

11   FFT, the faster version of discrete Fourier transform (DFT), calculates harmonics (amplitude, angle, and

12   harmonic order). The voltage waveform is not considered for FFT to reduce the complexity and calculation

13   time. Therefore, FFT is only applied to the current waveform, and the angle and amplitude for each harmonic

14   are obtained. Then, THDI is calculated by (6) [30], and THDSS, which is the SS of THD, is calculated by (7).

$$THD_I = \frac{\sqrt{\sum_{h=2}^{50} I_h^2}}{I_1} * 100. \tag{6}$$

$$THD_{ss} = \begin{cases} 100 * \frac{THD_{I-rc}}{THD_{I-u}}, & THD_{I-rc} < THD_{I-u}. \\ 100 * \frac{THD_{I-u}}{THD_{I-rc}}, & THD_{I-u} < THD_{I-rc}. \end{cases} \tag{7}$$

15   where, I_h is the harmonic current, and I_1 is the fundamental current. In multiple load cases, I_h is

16   obtained by the vectorial sum of the corresponding harmonic currents since they may not be in phase with

17   each other, and I_1 is obtained by the sum of the corresponding fundamental currents of loads. THD_{I-u} and

18   THD_{I-rc} are the THD_I for the unknown load and reconstructed load, respectively.

19   **4.4. Third Harmonic SS**

20   The third harmonic current is another layer for the identification process. The ratio of the third harmonic

21   (150Hz) to fundamental current (50Hz) depends on the load structure, as seen in Fig. 3 and Fig. 4. Fig. 3 is

22   a highly nonlinear characteristic load, and Fig. 4 is a linear characteristics load. As a result, (8) is adopted to

1   determine similarities between the measured load and the predicted one.

$$I_{ss-3} = \begin{cases} 100 * \frac{i_{3-rc}}{i_{3-u}}, & i_{3-rc} < i_{3-u}. \\ 100 * \frac{i_{3-u}}{i_{3-rc}}, & i_{3-u} < i_{3-rc}. \end{cases} \tag{8}$$

where i_{3-rc} is the vectorial sum of the corresponding third harmonic current of loads. i_{3-u} is the third harmonic current for the unknown load.

All steps are converted to an algorithm and presented below based on the evaluations.

1. Get measurements (time vs. current and voltage).

2. Extract one-period zero-crossing voltage and corresponding current from measurement.

3. Perform FFT for the current waveform.

4. Calculate the RMS current, third harmonic current, THDI, and power consumption.

5. Calculate the SSs for all features.

6. Pick all the load combinations with higher scores than 90 according to the scores for each feature.

7. Calculate the final scores from the selected load combination in the previous step.

8. Decide the one with the highest SS as the decision (final winner).

5. Experimental Results and Discussions

All experiments presented in Table 2 are performed with the proposed method. Remember that each type-test contains ten measurements, and there are 56 type-tests in total. As a result, 560 identifications are evaluated by the embedded system, which performs the algorithm, and results are obtained. These results present accurate loads of 53 type-tests (530 experiments). However, three type-tests, 10, 11, and 32, contain a varying number of incorrect results. When we investigate the results, type-test 32 has only one inaccurate result out of 10 measurements. In addition, type-test-10 has two failed results, and type-test-11 cannot be identified in any of the measurements. Therefore, all these failed predictions are deeply investigated.

5.1. Failed Predictions

Three type-tests have failed predictions, and the first one is the type-test-10. Although the exact combination of the type-test-10 is VC and MO (loads 1 and 5), the method determines it as VC and TV (loads 1 and 6) in two cases. As indicated, VC is the common load for all evaluations, but MO is misidentified as TV in two. Also, Table 3 presents the SSs of the correct and failed experiments of the corresponding type-test. Fig. 8 shows the current waveforms of measurement and reconstructed current waveforms, both correct and failed ones. Although MO and TV are completely different in harmonic distributions and power consumption, it should be considered load composition. Since the evaluations of combination loads are based on the reconstructed waveforms, it is noticed that the measured current is located between the reconstructed ones. Therefore, the result is declared type-test-11 instead of type-test-10 for the failed experiment with a tiny difference.

The second failed type-test is Type-test 11, consisting of VC and TV (loads 1 and 6). The load is identified as VC, HL, and MO (loads 1, 2, and 5) at the failed results. VC is the expected load for all results due to its relatively higher SS effect in the combination. However, TV cannot be determined in all experiments as TV. It is thought that the reason behind this situation is the measurement errors.

The last failed one is Type-test 32. Although it is a combination of HL, HE, and LC, one of the measurements is determined as HE, LC, and TV. As seen on the load combinations, HL is misidentified as TV. The reason is the same as the previous cases. As a result, there are only 13 failed predictions out of 560 experiments.

Table 2. Load tests.

Type-test*	Load	Type-test*	Load
1	VC	29	VC-LC-MO
2	HL	30	VC-LC-TV
3	HE	31	VC-MO-TV
4	LC	32	HL-HE-LC
5	MO	33	HL-HE-MO
6	TV	34	HL-HE-TV
7	VC-HL	35	HL-LC-MO
8	VC-HE	36	HL-LC-TV
9	VC-LC	37	HL-MO-TV
10	VC-MO	38	HE-LC-MO
11	VC-TV	39	HE-LC-TV
12	HL-HE	40	HE-MO-TV
13	HL-LC	41	LC-MO-TV
14	HL-MO	42	VC-HL-HE-LC
15	HL-TV	43	VC-HL-HE-MO
16	HE-LC	44	VC-HL-HE-TV
17	HE-MO	45	VC-HL-LC-MO
18	HE-TV	46	VC-HL-LC-TV
19	LC-MO	47	VC-HL-MO-TV
20	LC-TV	48	VC-HE-LC-MO
21	MO-TV	49	VC-HE-LC-TV
22	VC-HL-HE	50	VC-HE-MO-TV
23	VC-HL-LC	51	VC-LC-MO-TV
24	VC-HL-MO	52	HL-HE-LC-MO
25	VC-HL-TV	53	HL-HE-LC-TV
26	VC-HE-LC	54	HL-HE-MO-TV
27	VC-HE-MO	55	HL-LC-MO-TV
28	VC-HE-TV	56	HE-LC-MO-TV
* Each set contains ten measurements			
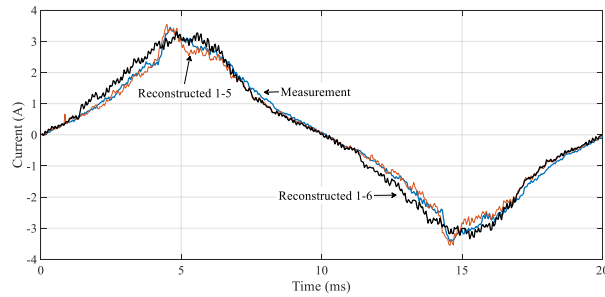
Figure 8. Harmonic analysis of MO & HL current.

5.2. Evaluations

To evaluate the success of the approach, accuracy (9), precision (10), recall (11), and F-score (12) metrics are employed.

Table 3. Correct and failed experiment results for type-test 10.

Correct Evaluation		Failed Evaluation	
Type-test	SS	Type-test	SS
10	**290.52**	**11**	**290.06**
11	**290.26**	**10**	**289.39**
9	196.43	9	196.6
47	98.73	47	99.44
25	98.10	25	97.74
23	97.22	23	96.53
29	95.44	29	95.51

$$Accuracy = \frac{Number\, of\, successful\, identification}{Number\, of\, experiments}. \tag{9}$$

$$Precision = \frac{TP}{TP + FP}. \tag{10}$$

$$Recall = \frac{TP}{TP + FN}. \tag{11}$$

$$F - score = 2 * \frac{precision * recall}{precision + recall}. \tag{12}$$

where TP, FN, and FP are true-positive (detected condition when the condition is present), false-negative (not detected condition when the condition is present), and false-positive (detected condition when the condition is absent), respectively.

Table 4. Performance results

	Accuracy	Precision	Recall	F-score
Individual load	100	1	1	1
Two loads	92.0000	0.9290	0.9600	0.9442
Three loads	99.5000	0.9983	0.9983	0.9983
Four loads	100	1	1	1
Total performance	97.6786	0.9853	0.9916	0.9884

The performance results are presented in Table 4. As can be seen in Table IV, an accuracy rate of 97.67% is obtained when considering all experiments. Furthermore, in all metrics, above ninety percent success is obtained. While the accuracy is about 97%, the precision and recall values are about 99%. It indicates that a significant portion of the loads in a combination are correctly determined, while one or two loads are misidentified. These results clearly show the success of the method. For single-load cases, it is indicated that all tests are accurately estimated. When the combinations consisting of different numbers of loads are evaluated separately, success of over 92% is achieved in all metrics. Table 5 is presented to compare the success of the proposed method with existing methods in the literature.

Table 5. Comparison of the proposed approach with existing methods in the literature

No	NILM Technique	Dataset	Accuracy	F-score
1	Du et al.[31]	WHITED	87.08	87.31
2	Liu et al.[32]	PLAID	80.70	78.71
3	Qu et al.[33]	WHITED	95.99	95.43
4	De Baets et al.[34]	PLAID	90.05	90.40
5	Proposed model	Laboratory prototype	97.67	98.84

In comparison, two base criteria called Accuracy and F-score metrics are used. As seen in Table 5, the proposed approach outperforms the selected studies in terms of both Accuracy and F-score. Due to factors such as the method used, measurement techniques, and the loads' characteristics, varying performances may be observed across different datasets. However, the results highlight the effectiveness of the proposed method.

6. Conclusion

This paper proposed a CDP method to determine any load/load combination in the system. THDI, RMS and third harmonic current, and power consumption are evaluated to identify loads. These electrical features obtained from high-frequency measurements (512 samples/period) have been considered for the study. In addition, this method contains a low-complexity algorithm that uses one-period current and voltage measurement.

The method is validated by six different loads and their fifty-six combinations. Each experimental test is repeated ten times, so there are ten measurements of each combination. As a result, 560 measurements are obtained, and 547 of them (97.67%) are perfectly identified. Remember that the rest of the inaccurate results (2.33%) include partly correct load determinations, as explained in the paper.

In the proposed method;

• A novel Competitive Decision Process is introduced for the first time in this study.

• A real-time STM-based embedded system is designed to perform the whole process.

• In all load combination cases, the total success rate of over 97% is achieved with all metrics.

• Waiting for any step changes and recording more than one-period data are eliminated since the method does not require a continuous measurement.

• Low power consumption loads can be disaggregated in most cases.

• Since only one-period measurements of single-load cases are required as references, a minimum database space is needed.

• The complexity of the approach is reduced by the proposed two-level process.

The future scope of the work will be to conduct in-depth research on demand-side management and system stability based on the dynamic model for conservation voltage reduction (CVR) studies since accurate load determination ensures a correct understanding of the load side.

References

[1] Hart G. Nonintrusive appliance load monitoring. Proceedings of the IEEE 1992; 80 (12): 1870-1891. https://doi.org/10.1109/5.192069

[2] Zeng W, Han Z, Xie Y, Liang R, Bao Y. Non-intrusive load monitoring through coupling sequence matrix reconstruction and cross stage partial network. Measurement 2023; 220: 113358. https://doi.org/10.1016/j.measurement.2023.113358

[3] Zhang Y, Lin C, Shao Z, Liu B. A non-intrusive identification method of harmonic source loads for industrial users. IEEE Transactions on Power Delivery 2022;37(5):4358-4369. https://doi.org/10.1109/TPWRD.2022.3168835

[4] Akarslan E, Dogan R. A novel approach for residential load appliance identification. Sustainable Cities and Society 2020; 63:102484. https://doi.org/10.1016/j.scs.2020.102484

[5] Rehman AU, Lie TT, Vall'es B, Tito SR. Event-detection algorithms for low sampling nonintrusive load monitoring systems based on low complexity statistical features. IEEE Transactions on Instrumentation and Measurement 2020; 69 (3): 751-759. https://doi.org/10.1109/TIM.2019.2904351

[6] Wu Z, Wang C, Xiong L, Li R, Wu T, Zhang H. A smart socket for real-time nonintrusive load monitoring. IEEE Transactions on Industrial Electronics 2023;70(10):10618–10627. https://doi.org/10.1109/TIE.2022.3224164

[7] Klemenjak C, Jost S, Elmenreich W. Yomopie: A user-oriented energy monitor to enhance energy efficiency in households. In: IEEE 2018 IEEE Conference on Technologies for Sustainability (SusTech); 2018. pp. 1-7. https://doi.org/10.1109/SusTech.2018.8671331

[8] Guo Z, Wang ZJ, Kashani A. Home appliance load modeling from aggregated smart meter data. IEEE Transactions on Power Systems 2015;30(1):254–262. https://doi.org/10.1109/TPWRS.2014.2327041

[9] Egarter D, Bhuvana VP, Elmenreich W. Paldi: Online load disaggregation via particle filtering. IEEE Transactions on Instrumentation and Measurement 2015;64(2):467–477. https://doi.org/10.1109/TIM.2014.2344373

[10] Ji TY, Liu L, Wang TS, Lin WB, Li MS, Wu QH. Non-intrusive load monitoring using additive factorial approximate maximum a posteriori based on iterative fuzzy c -means. IEEE Transactions on Smart Grid 2019;10(6):6667–6677. https://doi.org/10.1109/TSG.2019.2909931

[11] Wu X, Han X, Liu L, Qi B. A load identification algorithm of frequency domain filtering under current under determined separation. IEEE Access 2018;6:37094–107. https://doi.org/10.1109/ACCESS.2018.2851018

[12] Akbar M, Khan ZA. Modified nonintrusive appliance load monitoring for nonlinear devices. In: IEEE 2007 IEEE International Multitopic Conference; 2007. pp. 1-5. https://doi.org/10.1109/INMIC.2007.4557691

[13] Laughman C, Lee K, Cox R, Shaw S, Leeb S, Norford L, Armstrong P. Power signature analysis. IEEE Power and Energy Magazine 2003;1(2):56–63. https://doi.org/10.1109/MPAE.2003.1192027

[14] Zhou Z, Xiang Y, Xu H, Yi Z, Shi D, Wang Z. A novel transfer learning-based intelligent nonintrusive load-monitoring with limited measurements. IEEE Transactions on Instrumentation and Measurement 2021;70:1–8. https://doi.org/10.1109/TIM.2020.3011335

[15] Chen S, Zhao B, Zhong M, Luan W, Yu Y. Nonintrusive load monitoring based on self-supervised learning. IEEE Transactions on Instrumentation and Measurement 2023;72:1–13. https://doi.org/10.1109/TIM.2023.3246504

[16] Akarslan E, Dogan R. A novel approach based on a feature selection procedure for residential load identification. Sustainable Energy, Grids and Networks 2021;27:100488. https://doi.org/10.1016/j.segan.2021.100488

[17] Wu X, Guo Y, Yan M, Li X, Yao L, Gong G. Non-intrusive load monitoring using identity library based on structured feature graph and group decision classifier. IEEE Transactions on Smart Grid 2023;14(3):1958–1973. https://doi.org/10.1109/TSG.2022.3209213

[18] Huang G, Zhou Z, Wu F, Hua W. Physics-informed time-aware neural networks for industrial nonintrusive load monitoring. IEEE Transactions on Industrial Informatics 2023;19(6):7312–22. https://doi.org/10.1109/TII.2022.3211075

[19] SRamadan R, Huang Q, Bamisile O, Zalhaf AS. Intelligent home energy management using internet of things platform based on nilm technique. Sustainable Energy, Grids and Networks 2022;31:100785. https://doi.org/10.1016/j.segan.2022.100785

[20] Zhang F, Qu L, Dong W, Zou H, Guo Q, Kong Y. A novel nilm event detection algorithm based on different frequency scales. IEEE Transactions on Instrumentation and Measurement 2022;71:1–11. https://doi.org/10.1109/TIM.2022.3181897

14

[21] Kotsilitis S, Kalligeros E, Marcoulaki EC, Karybali IG. An efficient lightweight event detection algorithm for on-site non-intrusive load monitoring. IEEE Transactions on Instrumentation and Measurement 2023;72:1–13. https://doi.org/10.1109/TIM.2022.3232169

[22] . Li Y, Wang X, Xia Y, Sun L. Sparse bayesian technique for load identification and full response reconstruction. Journal of Sound and Vibration 2023;553:117669. https://doi.org/10.1016/j.jsv.2023.117669

[23] Yan L, Tian W, Han J, Li Z. Event-driven two-stage solution to non-intrusive load monitoring. Applied Energy 2022;311:118627. https://doi.org/10.1016/j.apenergy.2022.118627

[24] Ruoyuan Z, Ma R. Non-invasive load identification method based on abc-svm algorithm and transient feature. Energy Reports 2022;8:63–72. https://doi.org/10.1016/j.egyr.2022.10.075

[25] Le TTH, Kim H. Non-intrusive load monitoring based on novel transient signal in household appliances with low sampling rate. Energies 2018;11(12):3409. https://doi.org/10.3390/en11123409

[26] Tsai MS, Lin YH. Modern development of an adaptive non-intrusive appliance load monitoring system in electricity energy conservation. Applied Energy 2012;96:55–73. https://doi.org/10.1016/j.apenergy.2011.11.027

[27] Lin YH, Tsai MS. Development of an improved time–frequency analysis-based nonintrusive load monitor for load demand identification. IEEE Transactions on Instrumentation and Measurement 2014;63(6):1470–83. https://doi.org/10.1109/TIM.2013.2289700

[28] Chang HH, Lian KL, Su YC, Lee WJ. Power-spectrum-based wavelet transform for nonintrusive demand monitoring and load identification. IEEE Transactions on Industry Applications 2014;50(3):2081–2089. https://doi.org/10.1109/TIA.2013.2283318

[29] Dogan R, Akarslan E. Investigation of electrical characteristics of residential light bulbs in load modelling studies with novel similarity score method. IET Generation, Transmission & Distribution 2020;14(23):5364–5371. https://doi.org/10.1049/iet-gtd.2020.0674

[30] F II I. Ieee recommended practices and requirements for harmonic control in electrical power systems. New York, NY, USA 1993.

[31] Du L, He D, Harley RG, Habetler TG. Electric load classification by binary voltage–current trajectory mapping. IEEE Transactions on Smart Grid 2016;7(1):358–365. https://doi.org/10.1109/TSG.2015.2442225

[32] Liu H, Wu H, Yu C. A hybrid model for appliance classification based on time series features. Energy and Buildings 2019;196:112–123. https://doi.org/10.1016/j.enbuild.2019.05.028

[33] Qu L, Kong Y, Li M, Dong W, Zhang F, Zou H. A residual convolutional neural network with multi-block for appliance recognition in non-intrusive load identification. Energy and Buildings 2023;281:112749. https://doi.org/10.1016/j.enbuild.2022.112749

[34] De Baets L, Ruyssinck J, Develder C, Dhaene T, Deschrijver D. Appliance classification using vi trajectories and convolutional neural networks. Energy and Buildings 2018;158:32–6. https://doi.org/10.1016/j.enbuild.2017.09.087